Biosensors and Bioelectronics 78 (2016) 267–273

Contents lists available at ScienceDirect

Biosensors and Bioelectronics

journal homepage: www.elsevier.com/locate/bios

A plasmonic colorimetric strategy for biosensing through enzyme guided growth of silver nanoparticles on gold nanostars

Yuehua Guo, Jie Wu, Jie Li, Huangxian Ju *

State Key Laboratory of Analytical Chemistry for Life Science, School of Chemistry and Chemical Engineering, Nanjing University, Nanjing 210023, PR China

ARTICLE INFO

Article history:
Received 18 September 2015
Received in revised form
30 October 2015
Accepted 18 November 2015
Available online 28 November 2015

Keywords:
Surface plasmon resonance
Plasmonic colorimetric assay
Gold nanostars
Alkaline phosphatase
DNA
Silver nanoparticles

ABSTRACT

A plasmonic colorimetric strategy was designed for sensitive detection of biomolecules through enzyme guided silver nanoparticles (AgNPs) growth on gold nanostars (AuNS). The growth of AgNPs on AuNS led to a substantial blue shift of the localized surface plasmon resonance (LSPR) peak and the color change of AuNS from blue to dark blue, purple and ultimately orange. Both the LSPR blueshift wavelength and the color of detection solution containing AuNS, Ag^+ and ascorbic acid 2-phosphate (AAP) depend on the amount of enzyme that catalyzed the dephosphorylation of AAP to reduce Ag^+ on AuNS surface. Thus this strategy could be used for LSPR and naked-eye detections of both the enzyme such as alkaline phosphatase (ALP) and other biomolecules involved in biorecognition events using ALP as a tag. The LSPR detection method for ALP showed a linear range from 1.0 pM to 25 nM with a detection limit of 0.5 pM. Using DNA as a mode target molecule, this technique showed a detection range from 10 fM to 50 pM DNA with a detection limit of 2.6 fM through the convenient combination with hybridization chain reaction amplification. The proposed plasmonic colorimetric strategy could be extended as a general analytical platform for design of immunosensors and aptasensors with ALP as a label.

© 2015 Elsevier B.V. All rights reserved.

1. Introduction

Colorimetric detection has received considerable attention due to the low cost, simplicity and practicality (Guo et al., 2013; Zhou et al., 2014). By taking the advantages of a large number of novel nanomaterials, plenty of colorimetric biosensors based on different principles have been developed (Liu et al., 2013a; Saha et al., 2012; Song et al., 2011; Tram et al., 2014; Wang et al., 2014; Zhang et al., 2013a). For example, a series of colorimetric methods based on the aggregation of metal nanoparticles have been proposed for sensitive and convenient detection of glucose (Li et al., 2012), DNA (Ji et al., 2011; Liu et al., 2013b), metal ions (Lee et al., 2007a), cancer cells (Lu et al., 2010), and enzymes (Wang et al., 2013). However, the practical application of these strategies is limited, since the aggregation of metal nanoparticles is susceptible to some external factors, such as high ionic strength or other impurities, which influences the reproducibility and precision of these detection methods. Although some mimic enzymes such as nanomaterials and DNAzyme have also been used for colorimetric detection of DNA (Park et al., 2011; Shimron et al., 2011), protein (Gao et al., 2007; Gao et al., 2008), bacteria (Wan et al., 2012), cancer cell (Tao et al., 2013) and metal ions (Li et al., 2008), the design of novel colorimetric assay strategy to circumvent the drawbacks existing in the developed methods for their practical application still remains a significant challenge.

Recently, due to the unique tunable size, shape, composition, and plasmonic optical properties, noble metal nanoparticles have drawn particular interest in plasmonic sensing (De la Rica and Stevens, 2012; He et al., 2012; Liu et al., 2014; Xia et al., 2013; Xianyu et al., 2014; Yang et al., 2014). Enzymatic synthesis of nanoparticles in situ, which can improve significantly the signal to noise ratio, is the main way to regulate the size, shape, composition of nanoparticles (Pavlov, 2014). For example, the etching of gold nanorods has been employed for colorimetric glucose detection based on the cascade reaction of horseradish peroxidase and glucose oxidase (Saa et al., 2014), and the etching of triangular silver nanoprism can induce a substantial surface plasmon resonance shift, which leads to a method for DNA detection, though the peak shift is only about 40 nm in whole calibration range (He et al., 2012). The protruding tips of gold nanostars (AuNS), one of the anisotropic plasmonic gold nanostructures, have high electromagnetic field enhancements (Jana et al., 2015). Thus this nanostructure is attractive for localized surface plasmon resonance (LSPR) biosensing application. In a sandwich immunoassay format, the use of AuNS achieves a LSPR detection of attomole prostate-specific antigen (Lorenzo et al., 2012). This method uses glucose oxidase labeled to antibody to generate hydrogen peroxide for reduction of silver ions around AuNS, which yields a blueshift in

* Corresponding author.
E-mail address: hxju@nju.edu.cn (H. Ju).

http://dx.doi.org/10.1016/j.bios.2015.11.056
0956-5663/© 2015 Elsevier B.V. All rights reserved.

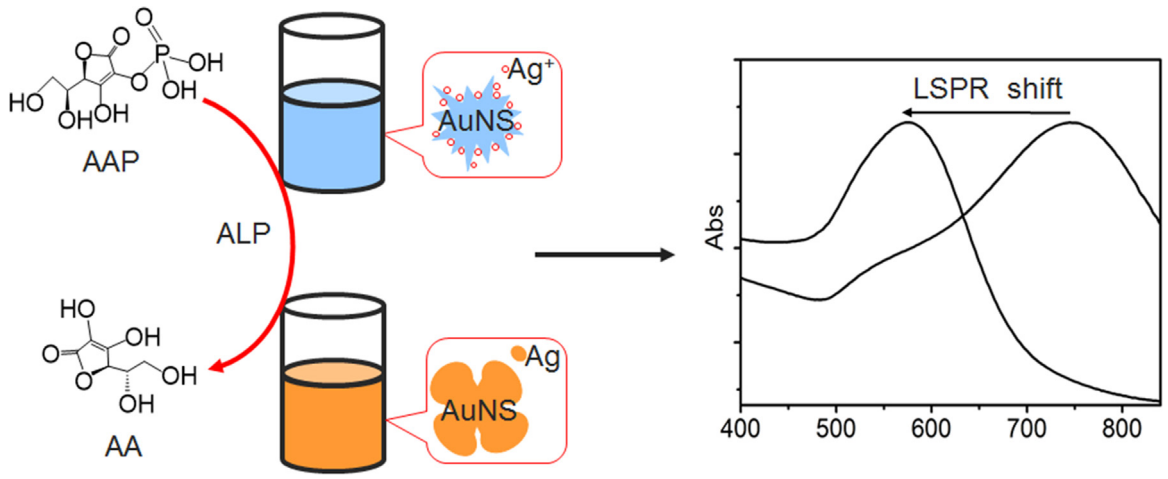

Scheme 1. Schematic representation of plasmonic colorimetric strategy for ALP detection via enzyme guided growth of AgNPs on AuNS and LSPR blueshift.

LSPR of AuNS. However, the formation of free-standing silver nanocrystals leads to inverse response and thus limits the detectable concentration range of analyte. Moreover, the alteration of solution parameters such as pH and precursor concentration can exert a huge impact on the response (Lorenzo et al., 2012), which also limits its practical application.

Inspired by the LSPR blueshift of AuNS due to the enzyme-guided growth of silver nanoparticles (AgNPs) (Lorenzo et al., 2012), this work designs a novel system for excluding the drawbacks mentioned above and performing the plasmonic colorimetric detection of both alkaline phosphatase (ALP) and DNA as a model analyte involved in biorecognition events. ALP is an important biomarker in clinical diagnosis such as adynamic bone disease, hepatitis and prostatic cancer (Zhou et al., 2014), meanwhile, its activity has a profound influence on the dephosphorylation process (Choi et al., 2007; Li et al., 2013). By means of the ALP-catalyzed dephosphorylation and the controllable reduction of silver ions by ascorbic acid (AA), the plasmonic colorimetric detection of ALP can be achieved in the presence of ascorbic acid 2-phosphate (AAP) and AuNS (Scheme 1).

The enzyme-guided growth of AgNPs on AuNS can induce the color change of AuNS from blue to dark blue, purple and ultimately orange, which leads to a method for detection of ALP by naked eye. Due to the multi-catalysis of ALP to produce the reductant AA and the high molar extinction coefficient of AgNPs on AuNS surface, the naked-eye detection shows wide and continuous color change and thus wide detectable concentration range. Furthermore, this system can be conveniently combined with both the developed signal amplification strategies and the biorecognition events by using ALP as a tag. Here, as a concept proof, DNA hybridization is selected as a biorecognition event, and hybridization chain reaction (HCR), which can carry out the polymerization of oligonucleotides into a long double-strand DNA (dsDNA) spontaneously in the presence of an initiator DNA (Dirks and Pierce, 2004; Xu et al., 2013), is used for signal amplification by using two hairpin DNA—biotinylated H1 and H2 and avidin-tagged ALP to achieve both LSPR and naked-eye detection of the target DNA (Scheme 2). These methods show high sensitivity and wide concentration. The plasmonic colorimetric assay strategy can also be extended for the design of immunosensors and aptasensors with ALP as a label, thus it provides a general analytical platform for simple detection of enzyme and other biomolecules involved in biorecognition events.

2. Materials and methods

2.1. Materials and reagents

Calf intestine ALP, poly(vinylpyrrolidone) (PVP, MW= 10,000), AAP, N-(3-dimethylamino-propyl)-N′-ethylcarbodiimide hydrochloride (EDC), silver nitrate ($AgNO_3$), monoethanolamine (MEA) and N-hydroxysuccinimide (NHS) were purchased from Sigma-Aldrich. Chloroauric acid ($HAuCl_4 \cdot 4H_2O$) was obtained from Shanghai Chemical Reagent Company (Shanghai, China). Trisodium citrate and N,N-dimethylformamide (DMF) were obtained

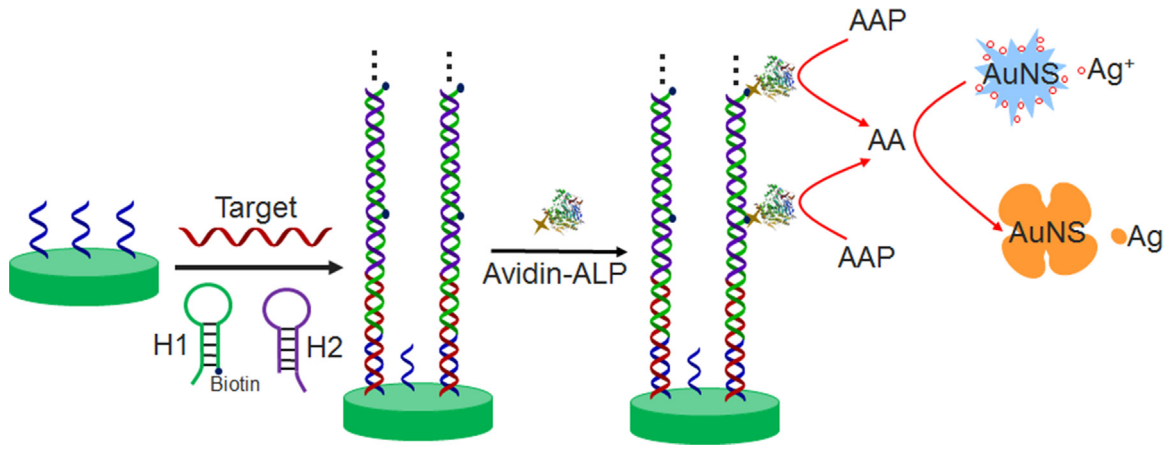

Scheme 2. HCR-based DNA detection with plasmonic colorimetric strategy.

from Sinopharm Chemical Reagent Co., Ltd. (China). Avidin-ALP and carboxyl-modified 96-well plate were purchased from Nanjing Olive Twigs Biotech. Co., LTd (Nanjing, China). Other chemicals were of analytical reagent grade and used as received. Ultrapure water obtained from a Millipore water purification system ($\geq$ 18 MΩ, Milli-Q, Millipore) was used in all assays. The oligonucleotides with the following sequences were purchased from Shanghai Sangon Biotechnology Co. Ltd. (China) and purified using high-performance liquid chromatography. Their sequences were as follows:

Capture probe: 5′-NH2-TATTAACTTTACTCC-3′

Hairpin probe H1: 5′-CTTCCTCCCCGCTGACAAAGTTCAGCGGGG-biotin-3′

Hairpin probe H2: 5′-TCAGCGGGGAGGAAGCCCCGCT-GAACTTTG-3′

Target DNA: 5′-TCAGCGGGGAGGAAGGGAGTAAAGTTAATA-3′

Single-base mismatch DNA: 5′-TCAGCGGGGAGGAAGGGAG-TAAAATTAATA-3′

Non-complementary sequences: 5′-GTGATCATACTTGGCAACT-CGGTACCGCGC-3′

2.2. Apparatus

Polyacrylamide gel electrophoresis (PAGE) analysis was performed on an electrophoresis analyzer (Liuyi Instrument Company, China) and imaged on Bio-rad ChemDoc XRS (Bio-Rad, USA). Transmission electronmicroscopic (TEM) images and energy dispersive x-ray analysis (EDAX) were recorded on a Model JEM 2100 highresolution TEM microscope (JEOL, Japan). Zeta potential analysis was performed on Zetasizer (Nano-Z, Malvern, UK). The ultraviolet–visible (UV–vis) absorption spectra were recorded with a Nanodrop-2000C UV–vis spectrophotometer (Nanodrop, USA). For DNA detection, the UV–vis absorption spectra were carried out on a Synergy hybrid 1 multimode microplate reader (BioTek).

2.3. PAGE analysis

A 5% native polyacrylamide gel was prepared using 5 × TBE buffer. The loading sample was the mixture of 7 μL DNA sample, 1.5 μL 6 × loading buffer, and 1.5 μL of UltraPowerTM dye. Before injection into the polyacrylamide hydrogel, the loading sample was placed for 3 min. The gel electrophoresis was run at 90 V for 1 h. The resulting board was illuminated with UV light and photographed with a Molecular Imager Gel Doc XR.

2.4. Synthesis of AuNS

Gold nanoparticles were firstly synthesized by adding 2.5 mL of 1 wt% trisodium citrate solution to 50 mL boiling solution of 0.5 mM $HAuCl_4$ according to previous report (Wheeler et al., 2012). The as-formed nanoparticles were then coated with PVP to obtain the seeds by adding 3.5 mL of 2.5 mM PVP and stirred overnight at room temperature. The solution was centrifuged and then dispersed in 5 mL ethanol.

82 μl of 50 mM $HAuCl_4$ was mixed with 15 mL DMF solution of 10 mM PVP, followed by rapid addition of 43 μL PVP-coated Au seeds in ethanol under stirring. Within 15 min, the color of the mixture changed from pink to colorless, and finally turned blue, indicating the formation of AuNS in solution (Kumar et al., 2008). The mixture was centrifuged (6000 rpm) and washed to remove excess PVP with ethanol at least five times. The obtained AuNS was finally dispersed in 2 mL ultrapure water with 0.05% Tween.

2.5. Detection of ALP and target DNA

The analysis of ALP was performed by simply adding ALP solution or sample in 80 μL Tris–HCl (pH 9.5) buffer containing 16 μL AuNS, 0.7 mM Ag^+, 4 mM AAP to incubate at 37 °C for 15 min, which was subjected to UV–vis measurement by scanning from 400 to 850 nm. The detection of DNA was performed in capture DNA modified 96-well plate, which was prepared by incubating NH_2-modified capture DNA (1 nM) in a carboxyl-modified 96-well plate that was firstly activated using 10 mM PBS (pH 5.5, 100 μL) containing 10 mM EDC and 20 mM NHS for 60 min at room temperature, and then blocking the active sites with 100 μL of 1 mM MEA for 2 h at 4 °C. After 50 μL target DNA or DNA sample was annealed by heating at 95 °C for 5 min and then slowly cooled down to room temperature, it was mixed with 50 μL H1 (500 nM) and 50 μL H2 (500 nM) in the capture DNA modified well to incubate for 1 h at room temperature, which formed dsDNA sequence through in situ HCR. After the well was washed, 10 μL avidin-ALP (2 μg/ml) was added and incubated for 1 h at room temperature. Lastly, the well was washed, and 100 μL Tris–HCl (pH 9.5) containing 24 μL AuNS, 0.7 mM Ag^+ and 10 mM AAP was added and incubated for 30 min at 37 °C to perform the UV–vis measurement by scanning from 400 to 900 nm.

3. Results and discussion

3.1. Feasibility of plasmonic colorimetric assay

The feasibility of the plasmonic colorimetric assay through ALP guided AgNPs growth on the surface of AuNS was investigated by several control experiments. As shown in Fig. 1, no appreciable color change was observed in the absence of AuNS, ALP, AAP or Ag^+. After incubation at 37 °C for 15 min, these solutions did not show any shift of LSPR peak. However, the solution containing all these components showed the significant color change of AuNS from blue to orange, which accompanied a large shift of LSPR peak (about 200 nm). This phenomenon could be attributed to the growth of AgNPs on the surface of AuNS (Scheme 1) and much higher extinction coefficient of AgNPs than AuNS (Lee et al., 2007b). In addition, the presence of AuNS could greatly enhance the ALP induced silver deposition reaction, which acted as seeds for silver growth. This indicated that silver growth was attributed to the enzyme mediated generation of AA. The whole reaction could be described by the following equations (Jang et al., 2015; Zhou et al., 2014).

$$AAP \xrightarrow{ALP} AA + PO_4^{3-}$$

$$AA + Ag^+ \xrightarrow{AuNS} DHA + 2Ag^0 + 2H^+$$

3.2. Characterization of growth of AgNPs on AuNS

The TEM image of the prepared PVP-capped AuNPs showed good distribution with an average diameter around 15 nm (Fig. S1A), which was further confirmed by DLS experiment showing an average hydration diameter of 16.2 nm (Fig. S1B). This result could be verified by UV–vis spectrum in which an absorption peak was observed at 520 nm (Fig. S1C). After reduced Au was deposited on the AuNPs as the seeds, the obtained AuNS showed a star-shaped morphology with a greater size and protruding tips (Fig. 2A). The yield of AuNS nanostructures was extremely high (practically 100%). Each nanostar showed a roughly spherical core and several pointed protrusions. The average particle radius was measured to be 55 ± 5 nm. The corresponding EDAX spectrum showed only the signals of Au at 2.11, 9.72 and 11.50 KeV, and no signal for Ag was observed (Fig. 2C). Upon the addition of 8 μL of 7 mM Ag^+ in 16 μL AuNS solution, the Zeta potential become more positive, indicating

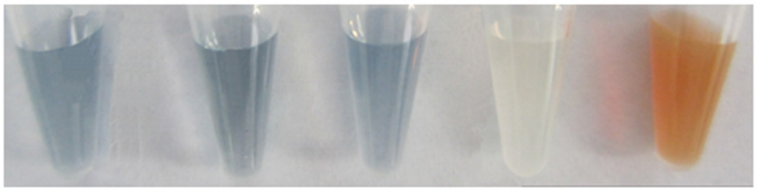

	Δλ= 0 nm	Δλ= 0 nm	Δλ= 0 nm	Δλ= 0 nm	Δλ= 200 nm
AuNS	√	√	√		√
AAP	√	√		√	√
Ag^+	√		√	√	√
ALP		√	√	√	√

Fig. 1. Feasibility of the enzyme-guided growth of AgNPs on AuNS. AAP: 4 mM, Ag^+: 7.0 mM, ALP: 25 nM, and pH: 9.5. (For interpretation of the references to color in this figure, the reader is referred to the web version of this article.)

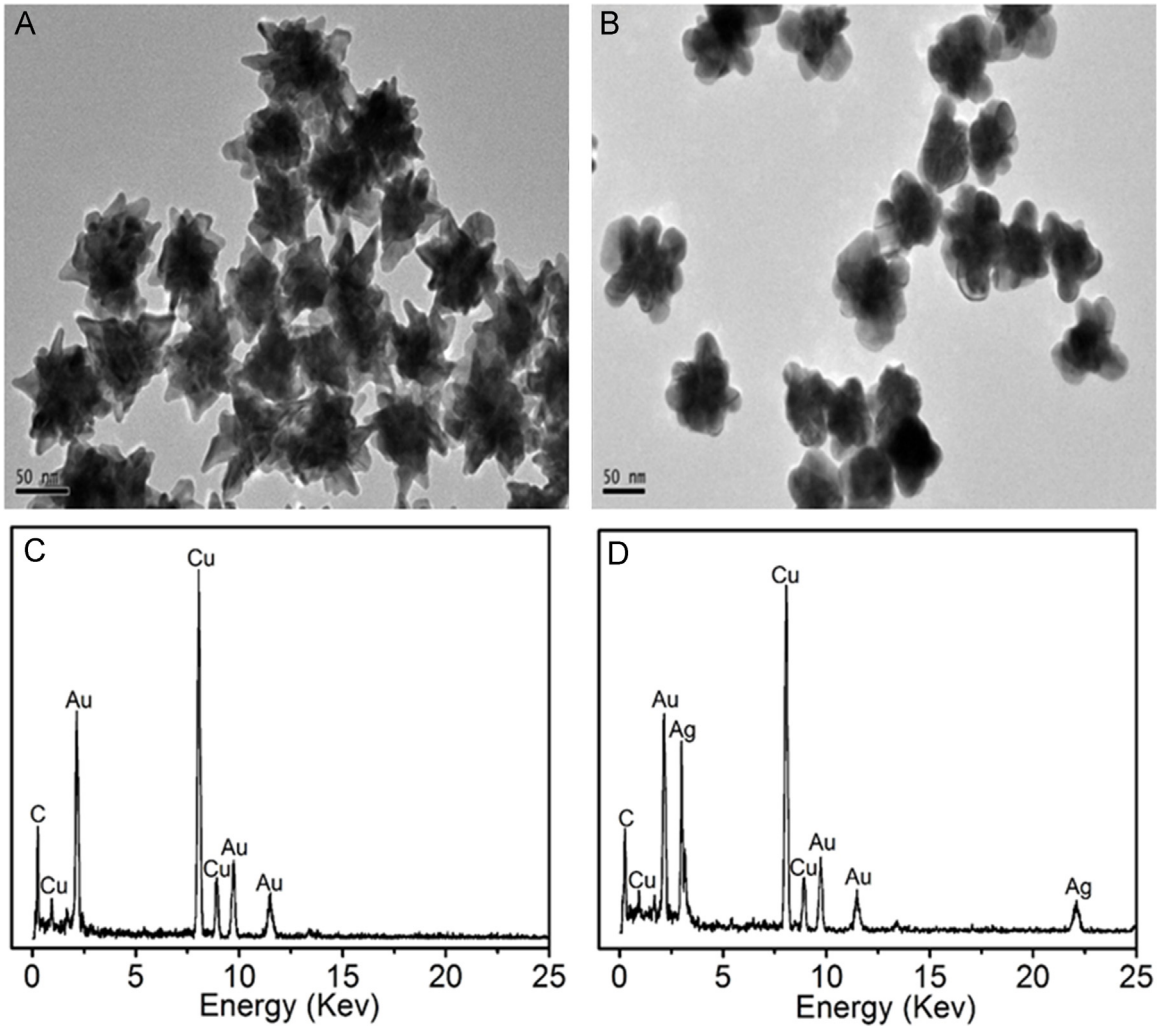

Fig. 2. TEM images of (A) AuNS and (B) AuNS coated with AgNPs, and corresponding EDAX spectra (C and D) detected with carbon-coated copper grids.

the adsorption of Ag^+ on AuNS due to its negatively charged surface (Fig. S2A), which led to strong electrostatic interaction between Ag^+ and AuNS surface. The addition of 8 μL 40 mM AAP did not change the morphology of AuNS (Fig. S2B). After 48 μL Tris–HCl (pH 9.5) buffer containing 25 nM ALP were added in this solution and incubated at 37 °C for 15 min, the pointed protrusions of AuNS disappeared and the morphology obviously changed into petal similar shape (Fig. 2B), indicating the growth of AgNPs on AuNS, which led to two strong EDAX peaks at 2.99 and 22.11 KeV (Fig. 2D). Thus the presence of the enzyme was crucial for the growth of AgNPs.

3.3. Optimization of detection conditions

It was clear that the LSPR peak shift originated from the growth of AgNPs. To achieve the excellent performance of plasmonic colorimetric assay for ALP analysis, several experiment parameters such as the concentrations of Ag^+ and AAP, and the incubation time for growth of AgNPs were optimized. The LSPR peak shift increased with the increasing Ag^+ concentration, which led to faster reduction reaction and more deposited AgNPs (Fig. S3A). At the Ag^+ concentration of 0.7 mM, the LSPR peak shift reached a maximum value, indicating that the further growth of AgNPs did not change the position of LSPR peak, which warranted the stability of the proposed analytical method and avoided the problem of inverse response reported previously (Lorenzo et al., 2012). Of course, the LSPR peak shift depended on the formation of AA intermediate generated by enzymatic hydrolysis of AAP substrate. With the increasing concentration of AAP, the LSPR peak shift increased and reached the maximum shift at 4 mM AAP (Fig. S3B). At the optimal Ag^+ and AAP concentrations, the LSPR peak shift increased with the increasing incubation time (Fig. S3C). The largest LSPR peak shift was obtained after 15 min, which was selected as the optimal reaction time.

3.4. ALP detection

Under optimal conditions, this system was applicable for ALP detection. As shown in Fig. 3A, the LSPR peak shifted when the concentration of ALP increased from 1 pM to 25 nM, demonstrating that the growth of AgNPs on the surface of AuNS was strongly dependent on the concentration of ALP, which decided the formation rate of AA intermediate. A semilogarithmic dependence of the blueshift of the LSPR peak on the concentration of ALP was shown in Fig. 3B, which represented the detectable range for ALP analysis. From the plot of peak shift vs the logarithmic value of ALP concentration, a detection limit of 0.5 pM was obtained at 3δ for LSPR peak measurement of blank solution. The detection limit was comparable to the assay based on ALP-catalyzed dephosphorylation (Xianyu et al., 2014), five times lower than traditional ELISA method (Gomez et al., 1995), and also 3–5 orders of magnitude lower than other metal nanoparticle based colorimetric methods (Choi et al., 2007; Wei et al., 2008; Zhao et al., 2007) and some fluorescent detection methods (Liu and Schanze, 2008; Zhang et al., 2013b).

It was noted that the color of the detection solution remained blue, the color of AuNS, in the absence of ALP, while the color changed from blue to dark blue, purple and ultimately orange as ALP concentration increased (Fig. 3C), which was contributed to the growth of AgNPs and the fact that more AgNPs were deposited on the surface of AuNS. As a consequence, the presence of ALP could be directly observed with the naked eye through the color change. The wide and continuous color change led to a wide distinguishable concentration range in the naked-eye detection.

3.5. DNA detection via biorecognition

Now that the LSPR peak shift depends on the amount of ALP, this strategy can be conveniently used for detection of other biomolecules by using ALP as a signal tag. Scheme 2 schematically

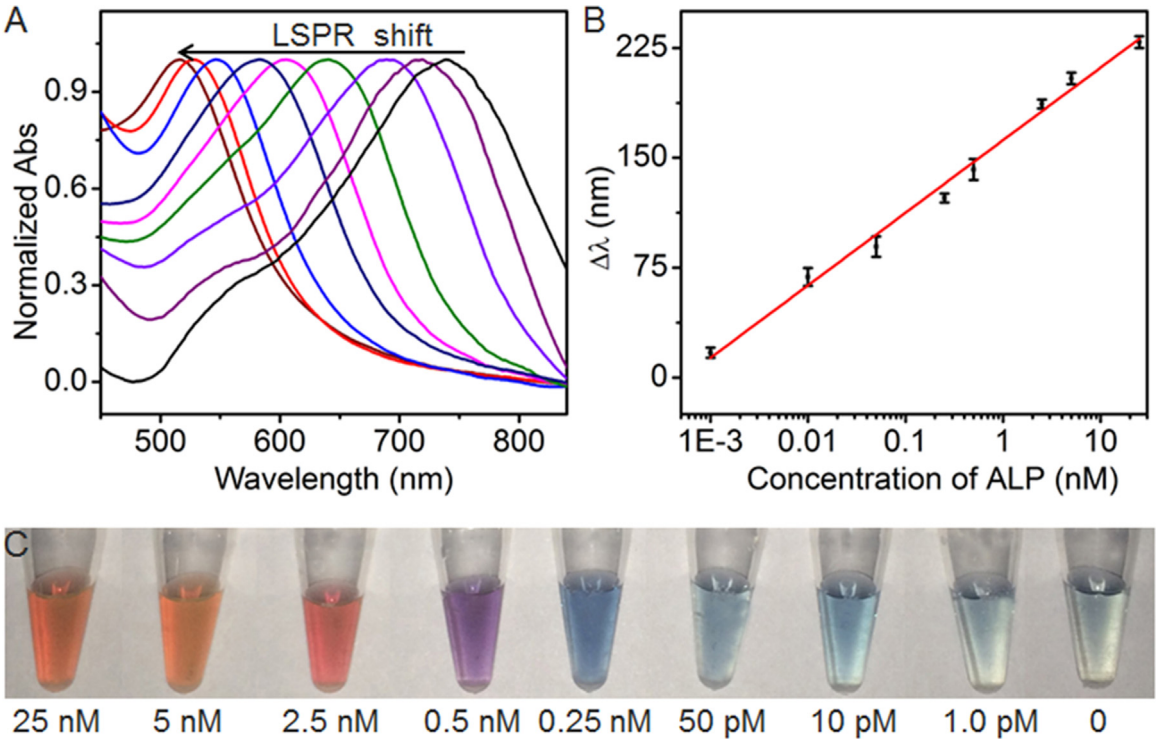

Fig. 3. (A) UV–vis spectra of the mixture of AuNS and AAP in presence of different concentrations of ALP, (B) plot of peak shift vs logarithm of ALP concentration, and (C) photograph for color change of detection solution upon incubation with ALP at marked concentration for 15 min. (For interpretation of the references to color in this figure, the reader is referred to the web version of this article.)

depicts a principle of plasmonic colorimetric assay for DNA analysis, which combines with a HCR for signal amplification. The HCR for DNA detection involves the self-assembly of target DNA and two hairpin DNA probes on capture DNA modified surface. Thus a carboxyl-modified 96-well plate was firstly activated via EDC/NHS method and modified with capture DNA. In the presence of target DNA, biotinylated H1 and H2, which are stable and do not hybridize each other, were added in the wells. The HCR self-assembly formed a dsDNA sequence with multi-sites of biotin. Thus avidin-tagged ALP could interact with the biotin sites in the linear structure. Upon addition of the detection solution and following incubation, Ag^+ was coated on the surface of AuNS, and ALP-catalyzed dephosphorylation produced AA intermediate to reduce the Ag^+, which led to the color change of AuNS and a substantial blueshift of LSPR.

To demonstrate the formation of the dsDNA sequence, gel electrophoresis was performed to reveal the relationship between the amount of formed long dsDNA and the concentration of target DNA. In the absence of target DNA, a well-defined band (lane 1) was observed (Fig. S4), which indicated that two hairpin DNA probes were stable. In the presence of target DNA, a long dispersed band was observed (lanes 2–8). Consistent with previous study (Chen et al., 2012; Yang et al., 2014), less amount of target DNA could form a longer DNA sequence with high molecular weight, a high concentration of the target DNA resulted in the assembly of a broad range of ds-DNA structures of different lengths, which might be due to the fact that the growth of the dsDNA triggered by the target DNA did not stop until the monomers were depleted.

The amounts of capture DNA for preparation of the 96-well plate and hairpin DNA probes for HCR greatly affected the LSPR peak shift. The optimal concentrations of capture DNA and hairpin DNA probes were 1 nM and 0.5 μM, respectively (Fig. S5). Under optimal conditions, the LSPR peak shifted with the increasing concentration of target DNA from 10 fM to 50 pM (Fig. 4A). The plot of the LSPR blueshift vs the logarithm of target DNA concentration showed a linearity (Fig. 4B), which led to a detection limit of 2.6 fM at 3δ for LSPR peak measurement in the absence of target DNA. As expected, the color of the detection solution changed from blue to orange with the increasing concentration of target DNA (Fig. 4C), demonstrating the feasibility of plasmonic colorimetric assay by the naked eye.

The specificity of plasmonic colorimetric assay for DNA analysis was verified with three different DNA sequences (Fig. S6A). The target DNA that perfectly matched capture DNA and half of H1 showed the largest LSPR peak shift. The sequence with single base mismatched capture DNA led to a 67% decrease of LSPR peak shift. The response of Random DNA was close to that obtained from blank solution. These results indicated that this plasmonic colorimetric assay possessed excellent capability to differentiate perfectly matched and mismatched DNA, demonstrating the excellent selectivity of this method.

4. Conclusions

This work proposes a plasmonic colorimetric assay method based on enzyme guided growth of AgNPs on the surface of AuNS. This strategy shows a proportional response of LSPR blueshift to ALP in a wide concentration range. The response is stable and can avoid the problem of previous inverse response. This method shows highly sensitivity for ALP detection, and can conveniently combine with biorecognition events to detect other biomolecules by using ALP as a signal tag. As a model analyte involved in biorecognition events, this technique has successfully been employed for DNA analysis by introduction of a HCR for signal amplification. Moreover, the color of AuNS in detection solution shows a wide and continuous change from blue to dark blue, purple and ultimately orange, and can be easily distinguished at a glance. Therefore the detection of analytes in a wide concentration range can be achieved by naked eye. The proposed plasmonic colorimetric strategy could also be extended as a general analytical platform for design of other biosensors with ALP as a label,

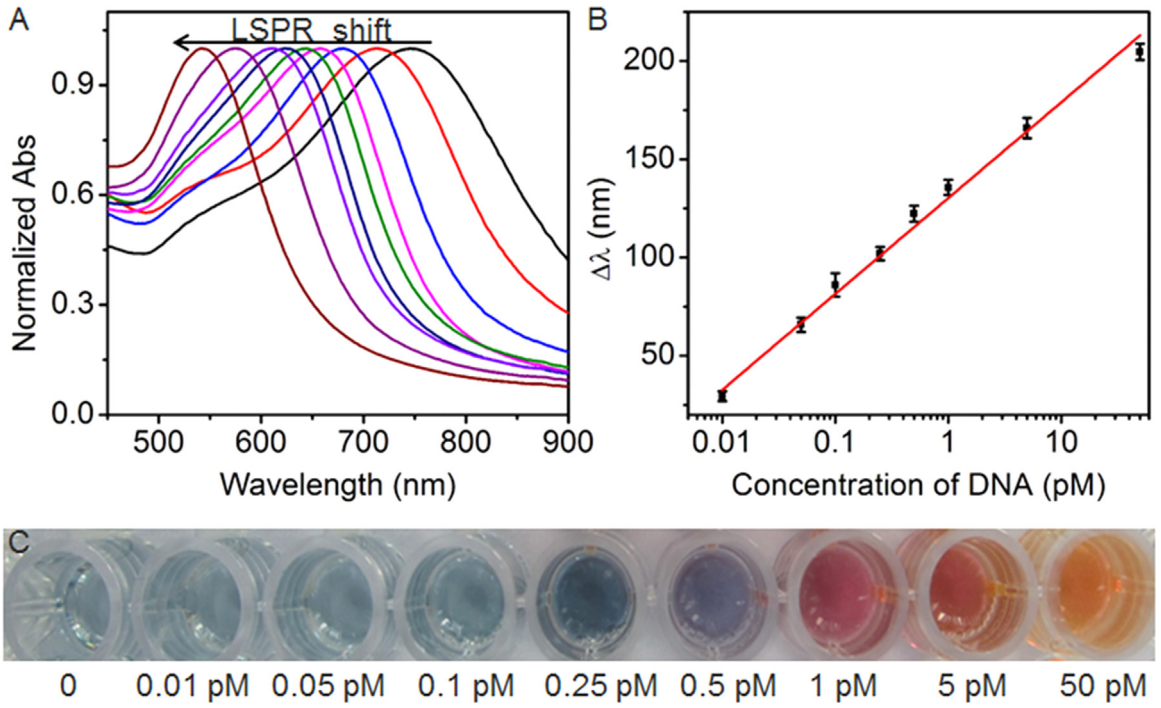

Fig. 4. (A) UV–vis spectra of the mixture of AuNS and AAP in capture DNA modified wells incubated with the mixtures of H1, H2 and different concentrations of DNA for 1 h and then avidin-ALP for 1 h, respectively. (B) Plot of peak shift vs logarithm of target DNA concentration, and (C) photograph of detection solutions at marked concentrations of DNA. (For interpretation of the references to color in this figure, the reader is referred to the web version of this article.)

showing a broad prospect in practical application.

Acknowledgments

We gratefully acknowledge the National Natural Science Foundation of China (21135002, 21121091, 21105046 and 21475063).

Appendix A. Supplementary material

Supplementary data associated with this article can be found in the online version at http://dx.doi.org/10.1016/j.bios.2015.11.056.

References

Chen, Y., Xu, J., Su, J., Xiang, Y., Yuan, R., Chai, Y.Q., 2012. Anal. Chem. 84, 7750–7755.
Choi, Y., Ho, N.H., Tung, C.H., 2007. Angew. Chem. Int. Ed. 46, 707–709.
De la Rica, R., Stevens, M.M., 2012. Nat. Nanotechnol. 7, 821–824.
Dirks, R.M., Pierce, N.A., 2004. Proc. Natl. Acad. Sci. USA 101, 15275–15278.
Gao, L.Z., Wu, J.M., Lyle, S., Zehr, K., Cao, L.L., Gao, D., 2008. J. Phys. Chem. C 112, 17357–17361.
Gao, L.Z., Zhuang, J., Nie, L., Zhang, J.B., Zhang, Y., Gu, N., Wang, T.H., Feng, J., Yang, D. L., Perrett, S., Yan, X.Y., 2007. Nat. Nanotechnol. 2, 577–583.
Gomez, B.J., Ardakani, S., Ju, J., Jenkins, D., Cerelli, M.J., Daniloff, G.Y., Kung, V.T., 1995. Clin. Chem. 41, 1560–1566.
Guo, L.H., Xu, Y., Ferhan, A.R., Chen, G.N., Kim, D.H., 2013. J. Am. Chem. Soc. 135, 12338–12345.
He, H.L., Xu, X.L., Wu, H.X., Jin, Y.D., 2012. Adv. Mater. 24, 1736–1740.
Jana, D., Matti, C., He, J., Sagle, L., 2015. Anal. Chem. 87, 3964–3972.
Jang, H.J., Ahn, J., Kim, M.G., Shin, Y.B., Jeun, M., Cho, W.J., Lee, K.H., 2015. Biosens. Bioelectron. 64, 318–323.
Ji, H.X., Dong, H.F., Yan, F., Lei, J.P., Ding, L., Gao, W.C., Ju, H.X., 2011. Chem. Eur. J. 17, 11344–11349.
Kumar, P.S., Pastoriza-Santos, I., Rodríguez-Gonzalez, B., Abajo, F.J.G.D., Liz-Marzan, L.M., 2008. Nanotechnology 19, 015606.
Lee, J.S., Han, M.S., Mirkin, C.A., 2007a. Angew. Chem. Int. Ed. 46, 4093–4096.
Lee, J.S., Lytton-Jean, A.K.R., Hurst, S.J., Mirkin, C.A., 2007b. Nano Lett. 7, 2112–2115.
Li, C.M., Zhen, S.J., Wang, J., Li, Y.F., Huang, C.Z., 2013. Biosens. Bioelectron. 43, 366–371.
Li, D., Wieckowska, A., Willner, I., 2008. Angew. Chem. Int. Ed. 47, 3991–3995.
Li, W., Feng, L.Y., Ren, J.S., Wu, L., Qu, X.G., 2012. Chem. Eur. J. 18, 12637–12642.
Liu, D.B., Wang, Z.T., Jin, A., Huang, X.L., Sun, X.L., Wang, F., Yan, Q., Ge, S.X., Xia, N.S., Niu, G., Liu, G., Hight Walker, A.R., Chen, X.Y., 2013a. Angew. Chem. Int. Ed. 52, 14065–14069.
Liu, D.B., Yang, J., Wang, H.F., Wang, Z.L., Huang, X.L., Wang, Z.T., Niu, G., Hight Walker, A.R., Chen, X.Y., 2014. Anal. Chem. 86, 5800–5806.
Liu, P., Yang, X.H., Sun, S., Wang, Q., Wang, K.M., Huang, J., Liu, J.B., He, L.L., 2013b. Anal. Chem. 85, 7689–7695.
Liu, Y., Schanze, K.S., 2008. Anal. Chem. 80, 8605–8612.
Lu, W.T., Arumugam, R., Senapati, D., Singh, A.K., Arbneshi, T., Khan, S.A., Yu, H.T., Ray, P.C., 2010. ACS Nano 4, 1739–1749.
Lorenzo, L.R., Rica, R.D.L., Álvarez-Puebla, R.A., Liz-Marzán, L.M., Stevens, M.M., 2012. Nat. Mater. 11, 604–607.
Park, K.S., Kim, M.I., Cho, D.Y., Park, H.G., 2011. Small 7, 1521–1525.
Pavlov, V., 2014. Part. Part. Syst. Charact. 31, 36–45.
Saa, L., Coronado-Puchau, M., Pavlov, V., Liz-Marzán, L.M., 2014. Nanoscale 6, 7405–7409.
Saha, K., Agasti, S.S., Kim, C.Y., Li, X.N., Rotello, V.M., 2012. Chem. Rev. 112, 2739–2779.
Shimron, S., Wang, F., Orbach, R., Willner, I., 2011. Anal. Chem. 84, 1042–1048.
Song, Y.J., Wei, W.L., Qu, X.G., 2011. Adv. Mater. 23, 4215–4236.
Tao, Y., Lin, Y.H., Huang, Z.Z., Ren, J.S., Qu, X.G., 2013. Adv. Mater. 25, 2594–2599.
Tram, K., Kanda, P., Salena, B.J., Huan, S.Y., Li, Y.F., 2014. Angew. Chem. Int. Ed. 53, 12799–12802.
Wan, Y., Zhang, D., Wu, J.J., Wang, Y., 2012. Biosens. Bioelectron. 33, 69–74.
Wang, F., Liu, X.Q., Lu, C.H., Willner, I., 2013. ACS Nano 7, 7278–7286.
Wang, L.D., Tram, K., Ali, M.M., Salena, B.J., Li, J.H., Li, Y.F., 2014. Chem. Eur. J. 20, 2420–2424.
Wei, H., Chen, C.G., Han, B.Y., Wang, E.K., 2008. Anal. Chem. 80, 7051–7055.
Wheeler, D.A., Green, T.D., Wang, H.N., Fernández-López, C., Liz-Marzán, L., Zou, S.L., Knappenberger, K.L., Zhang, J.L., 2012. Chem. Phys. Lett. 543, 127–132.
Xia, Y.S., Ye, J.J., Tan, K.H., Wang, J.J., Yang, G., 2013. Anal. Chem. 85, 6241–6247.
Xianyu, Y.L., Wang, Z., Jiang, X.Y., 2014. ACS Nano 8, 12741–12747.
Xu, J., Wu, J., Zong, C., Ju, H.X., Yan, F., 2013. Anal. Chem. 85, 3374–3379.
Yang, X.J., Yu, Y.B., Gao, Z.Q., 2014. ACS Nano 8, 4902–4907.
Zhang, L., Lei, J.P., Liu, L., Li, C.F., Ju, H.X., 2013a. Anal. Chem. 85, 11077–11082.
Zhang, L.L., Zhao, J.J., Duan, M., Zhang, H., Jiang, J.H., Yu, R.Q., 2013b. Anal. Chem. 85, 3797–3801.
Zhao, W., Chiuman, W., Lam, J.C.F., Brook, M.A., Li, Y.F., 2007. Chem. Commun. 36, 3729–3731.
Zhou, C.H., Zhao, J.Y., Pang, D.W., Zhang, Z.L., 2014. Anal. Chem. 86, 2752–2759.